IOP Publishing Measurement Science and Technology
Meas. Sci. Technol. **27** (2016) 025702 (11pp) doi:10.1088/0957-0233/27/2/025702

Ramp-hold relaxation solutions for the KVFD model applied to soft viscoelastic media

HongMei Zhang[1,2], **Yue Wang**[2,3] **and Michael F Insana**[2,4]

[1] Key Laboratory of Biomedical Information Engineering, Ministry of Education, School of Life Science and Technology, Xi'an Jiaotong University, Xianning West Road No.28, Xi'an, Shaanxi, 710049, People's Republic China
[2] Department of Bioengineering and Beckman Institute for Advanced Science and Technology, University of Illinois at Urbana-Champaign, Urbana, IL 61801, USA

E-mail: mfi@illinois.edu and claramei@mail.xjtu.edu.cn

Received 25 September 2015, revised 18 November 2015
Accepted for publication 30 November 2015
Published 11 January 2016

Abstract

The standard step-hold load-relaxation profile can yield variable estimates of mechanical properties due to the difficulty in achieving a step strain experimentally. A ramp-hold profile overcomes this limitation if appropriate model functions can be derived. Utilizing Boltzmann hereditary integral operators for two indentation geometries, analytical ramp solutions for load-relaxation were developed based on the Kelvin–Voigt fractional derivative (KVFD) model. The results identify three model parameters for characterizing viscoelastic behavior from a single model curve fit to the data: the elastic modulus E_0, fractional-order parameter α, and relaxation time constant τ. The quantitative nature of the analysis was validated through measurements on gelatin emulsion samples exhibiting viscoelastic behavior. KVFD-model-based solutions provide mathematically simple and experimentally flexible descriptions of load-relaxation behavior for a range of viscoelastic properties and experimental conditions; e.g. one closed-form solution can fit the ramp and the hold phases of the relaxation time series. Experiments show that the solution for a spherical indenter and plate compressor each fit well to the corresponding experimental relaxation curves with a coefficient of determination $R^2 > 0.98$. Parameters obtained from the spherical-tip indentation and plate-compression geometries agree within one standard deviation, confirming that the ramp solution based KVFD model yields consistent measurements for characterizing viscoelastic materials.

Keywords: mechanical properties, spherical indentation, plate compression, ramp-hold relaxation, soft polymer emulsion

(Some figures may appear in colour only in the online journal)

1. Introduction

Indentation is a primary modality for characterizing the mechanical properties of a large variety of materials. The load-relaxation curve obtained during a displacement/strain-hold experiment can reveal intrinsic properties of a viscoelastic material when an appropriate model is fit to the data [1, 2]. Exponential parameters from a Prony series applied to a load-relaxation curve are frequently considered in polymer characterizations [3], while the mechanics community prefers classical constitutive models such as the Maxwell model [4–6], the Kelvin–Voigt model [7–9] and standard linear solid models [10–12]. Combinations of these elementary models have also been applied to improve model fits while estimating viscoelastic parameters [13–15]. One common element of all these modeling approaches is to find a good balance between model simplicity and experimental fitting accuracy. Increasing

[3] Co-first author
[4] Author to whom all correspondence should be addressed.

the parametric dimension generally renders better fits, but increases the difficulty of translating model parameters into a concise set of intrinsic mechanical properties.

Fractional-derivative (FD) models have been applied in part to solve this dilemma. FD models represent viscoelastic material responses more closely than integer-order models and with fewer parameters [16–19]. Fractional-derivative models are a combination of spring and fractional-order dashpot elements that reflects both elastic and time-dependent viscous mechanical behavior. The model fits load-relaxation data well despite a small number of fit parameters. Fractional Maxwell model, fractional Kelvin–Voigt (KVFD) model and fractional standard linear solid models have been widely used to describe the mechanical response of a variety of biological tissues as well as tissue-mimicking phantoms [20–25]. As for modeling load-relaxation curves, KVFD was shown to represent soft polymer dynamics very well, and the corresponding model parameters have been interpreted in terms of the material properties of elasticity and viscosity [25].

A majority of load-relaxation tests apply step compressions mainly for the analytical convenience of deriving a step-hold relaxation response solution. However, it is difficult to apply a near-step strain without creating oscillating transients that are more representative of the measurement device than the material. Unless the transients are accurately modeled, significant errors in model parameters are generated. In contrast, the ramp-hold relaxation experiment dramatically improves model-fit stability by not generating measurement artifacts [26–29]. The analytical solution for the ramp-hold experiment can be derived by combining the Boltzmann integral with the constitutive equation of a given model assuming a closed-form integral formula can be found. Recently, Mattice *et al* [28] proposed a method based on a generalized Maxwell–Arm Wiechert model where no analytical solution was available for spherical-indentation testing. Instead, a correction factor was applied analogous to that of the ramp-hold applied stress solution for a creep experiment to correct fitted parameters from a step solution. The analysis demonstrated the feasibility and advantages of using ramp-hold applied strains to perform load-relaxation tests [28].

In this report, we explore models for estimating viscoelastic properties using the ramp-hold relaxation paradigm. Integer-order models expressed as Prony-series are compared to fractional-order expressions based on the Kelvin–Voigt material model. Performance of the analytical solution in describing the time-dependent mechanical response was examined using soft viscoelastic polymers with systematically varied viscosity. We studied the effects of different experimental conditions on KVFD parameter estimations; e.g. we varied the duration of the relaxation time series included in the model fits, the strain rates of the applied ramp deformations, and we compared measurements using spherical indention with those of plate compression. Results are evaluated based on estimation precision and measurement independence. Conclusions and recommendations for experimental protocols using the ramp-hold relaxation test are offered.

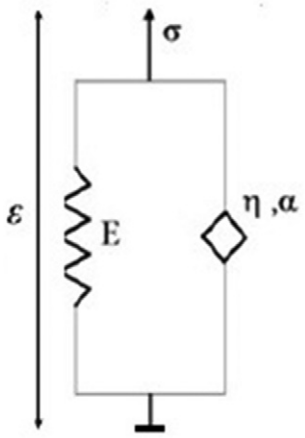

Figure 1. Schematic representation of the KVFD model.

2. Theory

2.1. KVFD model

The Kelvin–Voigt fractional derivative (KVFD) model describes the time-dependent relaxation behavior of viscoelastic materials. Strengths of this model include its flexibility for describing different types of materials with just three parameters. The linear KVFD model is illustrated in figure 1.

Stress σ is predicted from the applied strain ε given the relaxation modulus G of the material through the Boltzmann superposition integral [29, 30],

$$\sigma(t) = \int_{-\infty}^{t} G(t-\tau)\frac{\mathrm{d}\varepsilon(\tau)}{\mathrm{d}\tau}\mathrm{d}\tau. \tag{1}$$

For the KVFD model, the constitutive equation for the stress–strain relationship can be expressed by the following fractional-derivative equation [31]

$$\sigma(t) = E_0\varepsilon(t) + \eta\frac{\mathrm{d}^\alpha\varepsilon(t)}{\mathrm{d}t^\alpha} = E_0\left(\varepsilon(t) + \tau^\alpha\frac{\mathrm{d}^\alpha\varepsilon(t)}{\mathrm{d}t^\alpha}\right), \tag{2}$$

where E_0 is the elastic modulus, η is a viscosity coefficient, and α is a real number between (0,1) that defines the derivative order. Letting $\eta = E_0\tau^\alpha$, the relaxation time constant τ is used in place of η to give the second form of equation (2) to define a 3D feature set for materials characterization (E_0, α, τ).

The Laplace transforms of equations (1) and (2) can be equated to show the relaxation modulus for the KVFD model is

$$G(t) = E_0\left(1 + \frac{(t/\tau)^{-\alpha}}{\Gamma(1-\alpha)}\right), \tag{3}$$

where $\Gamma(z) = \int_0^\infty \mathrm{e}^{-t}t^{z-1}\mathrm{d}t$ is a Gamma function.

In the following sections, we derive a mathematical solution for the ramp-hold relaxation test based on the KVFD model for both the spherical-indenter and plate-compressor geometries. These are the analytic solutions fit to relaxation time series, including the ramp deformation, to estimate the 3D feature set.

2.2. Spherical indenter, ramp-hold relaxation solution

A hemi-spherical indentation tip is pressed into the surface of a large-size sample at constant velocity, after which the probe position is held fixed as we monitor relaxation of the force on the probe over time.

A force–displacement relation is used in place of a stress–strain relation modeling spherical indentation data. The Boltzmann integral expression for spherical indentation under displacement control was shown to be [28]

$$P(t) = \frac{8\sqrt{R}}{3}\int_0^t G(t-\tau)\frac{\mathrm{d}h^{3/2}(\tau)}{\mathrm{d}\tau}\mathrm{d}\tau, \tag{4}$$

where $P(t)$ is the force and $h(t)$ is the displacement depth of the indenter tip into the sample. The ramp-hold displacement function is

$$h(t) = \begin{cases} kt, & 0 \leqslant t \leqslant T_r \\ h_{\max} = kT_r, & t \geqslant T_r, \end{cases} \tag{5}$$

where T_r is the duration of the ramp and k is the velocity of the indenter tip during that time.

The time-varying force response predicted to occur during the ramp-hold relaxation test is derived by combining equations (3)–(5),

$$P_r(t) = \begin{cases} 4\sqrt{R}k^{3/2}E_0t^{3/2}\left[\dfrac{2}{3} + \dfrac{(t/\tau)^{-\alpha}}{\Gamma(1-\alpha)}B\left(\dfrac{3}{2}, 1-\alpha\right)\right], & 0 < t \leqslant T_r \\ 4\sqrt{R}k^{3/2}E_0T_r{}^{3/2}\left[\dfrac{2}{3} + \dfrac{\left(\frac{t}{T_r}\right)^{3/2}\left(\frac{t}{\tau}\right)^{-\alpha}}{\Gamma(1-\alpha)}B\left(\dfrac{T_r}{t}; \dfrac{3}{2}, 1-\alpha\right)\right], & t \geqslant T_r \end{cases} \tag{6}$$

where $B(x,y) = \int_0^1 t^{x-1}(1-t)^{y-1}\mathrm{d}t \qquad \mathrm{Re}(x) > 0, Re(y) > 0$ is a complete beta function and $B(a;x,y) = \int_0^a t^{x-1}(1-t)^{y-1}\mathrm{d}t$ for $a \in [0,1]$ is an incomplete beta function.

The step-hold displacement function is $h(t) = h_{\max}u(t)$, where $u(t)$ is the unit step function. So equation (1) reduces to

$$P(t) = \frac{8\sqrt{R}}{3}E_0h^{3/2}_{\max}\left(1 + \frac{(t/\tau)^{-\alpha}}{\Gamma(1-\alpha)}\right) \quad \text{for } t > 0. \tag{7}$$

A detailed derivation is provided in the appendix.

2.3. Plate compression, ramp-hold relaxation solution

In this experiment, a plate larger than the sample surface compresses a cylindrical sample from above and we assume free-slip boundary conditions. The sample is placed on a flat immovable surface with its side boundaries free to expand. A ramp displacement compresses the sample and is held fixed as the force on the plate is measured over time.

The time-dependence of the ramp-hold strain function is similar to equation (5), except that the strain $\varepsilon(t)$ is used instead of displacement $h(t)$. Using the Boltzmann integral expression from equation (1), the stress-relaxation response for the plate compressor is [29]

$$\sigma_r(t) = \begin{cases} \dfrac{\varepsilon_0E_0t}{T_r}\left[1 + \dfrac{(t/\tau)^{-\alpha}}{\Gamma(2-\alpha)}\right], & 0 \leqslant t \leqslant T_r \\ \dfrac{\varepsilon_0E_0}{T_r}\left[T_r - (t-T_r)\dfrac{((t-T_r)/\tau)^{-\alpha}}{\Gamma(2-\alpha)} + t\dfrac{(t/\tau)^{-\alpha}}{\Gamma(2-\alpha)}\right], & t > T_r \end{cases}. \tag{8}$$

The step-hold strain function is $\varepsilon(t) = \varepsilon_0\,u(t)$, which reduces equation (1) to

$$\sigma(t) = \varepsilon_0E_0\left(1 + \frac{(t/\tau)^{-\alpha}}{\Gamma(1-\alpha)}\right). \tag{9}$$

3. Materials and methods

3.1. Materials

The viscoelastic samples in this experiment are made of gelatin powder, deionized water and a skin cream each in specific weight percentages. Gelatin powder (Type B, Rousselot Inc., Dubuque IA) was mixed with deionized water in a beaker at room temperature, and heated in a 70 °C water basin for 45 min. The beaker was covered by aluminum foil to prevent water evaporation. It was stirred every 5 min until visually clear. After the gelatin–water mixture was removed from the water bath, it was cooled at room temperature to 30 °C, cream was added and stirred well until visibly homogeneous, and then the mixture is poured into cylindrical molds to congeal. The cylindrical mold is precisely machined to ensure a high degree of axial symmetry and flat, parallel end surfaces. Since samples retain their shape after being removed from the mold, they present a flat parallel surface to the plate compressor.

Cream (Vanicream, Pharmaceutical Specialties, Inc. Rochester, MN) was added to the molten gelatin as water was removed and the gelatin concentration held fixed in order to increase the viscosity of the sample without significantly changing stiffness. This gel–cream mixture is a solidified emulsion of cream particles suspended in liquid gelatin that is allowed to congeal into a solid. These samples express viscoelastic properties in the range of soft biological tissues. In contrast, gelatin gels constructed without the cream particles generally respond elastically to compression [36]. The molds used to form samples for spherical indentation testing are 50 mm in diameter and 20 mm in height. The molds used to form samples for plate testing are 37.5 mm in diameter and 19 mm in height. All samples were covered with plastic wrap and stored at room temperature for 16 h after construction and before mechanical testing. It is very important that the sample-manufacturing process be exactly reproduced in detail for material properties to be reproducible day to day.

Three different samples were prepared with the same gelatin concentrations (5% by weight). The concentrations of cream were 5%, 15%, and 50% by weight, and the corresponding deionized water concentrations were 90%, 80%, and 45%, respectively. These three samples are labeled Gel5Cream5, Gel5Cream15, and Gel5Creal50 in the results section.

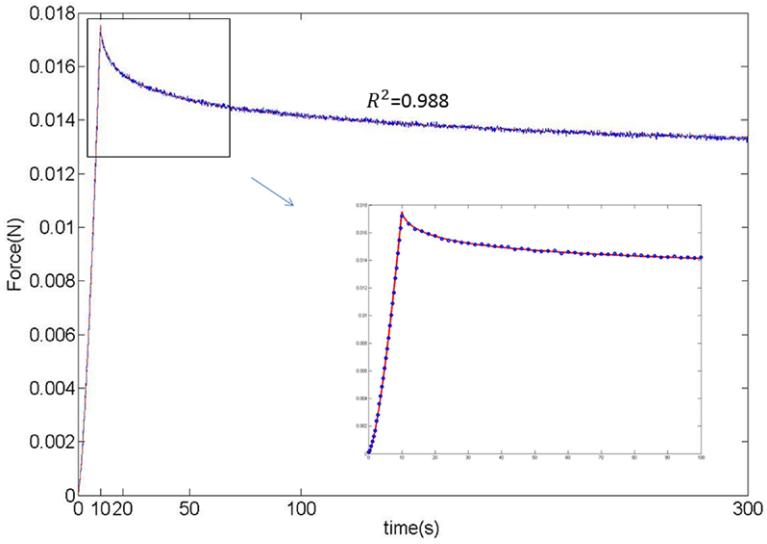

Figure 2. KVFD fitting of a measured ramp-hold relaxation curve for 5Gel5Cream sample using spherical indentation. The measured force-relaxation curve is shown as blue dots and the best-fit model curve is shown as a red dotted line. The experimental data in the zoomed figure is down sampled a factor of 10 in the ramp phase and 50 in the holding phase.

Table 1. KVFD model parameters estimated from different durations of the relaxation data (top row) for the 5Gel15Cream sample using spherical indentation. Values shown are from measurements made on one sample.

Time (s)	0–20	0–50	0–100	0–300	10–20	10–50	10 –100	10–300	CV1	CV2
E_0 (Pa)	2038.2	2032.1	2027.8	2021.3	2109.9	2096.2	2077.6	2068.1	0.0035	0.009
α	0.134	0.135	0.135	0.135	0.133	0.135	0.135	0.135	0.0037	0.0037
τ (s)	28.388	29.292	29.792	30.192	19.292	22.692	25.692	29.092	0.0264	0.1730

Note: CV1 values are coefficients of variation for fits including the ramp phase of the relaxation curve. CV2 values do not include the initial 10 s ramp phase.

3.2. Experiment

Mechanical testing employed the TA-XTPlus Texture Analyzer with two compression probes: a spherical-tipped indenter with 5 mm diameter and a flat plate compressor having a diameter larger than the cylindrical samples. Load-relaxation tests with ramp deformations were performed on each sample at room temperature.

The spherical indenter has a diameter one tenth that of the sample diameter to minimize boundary effects. The maximum displacement of the spherical probe into the top surface of the sample was always $h_{\max} = 1$ mm. However, the probe speed was varied between 0.01–5.0 mm s^{-1} to give a range of ramp times. Afterward, the probe was held in place for 200–300 s while the decaying force on the probe from viscous relaxation was measured. All tests were conducted with deionized water on top of the samples to minimize surface adhesion forces. We verified that water was not significantly absorbed by the samples during the experiments, and thus the mechanical properties of the phantom were not significantly influenced by the water. Specifically, force–displacement measurements made with water on the top sample surface and processed according to Hertzian contact theory to find an elastic modulus were found to be equivalent to force–displacement measurements made without water on the sample and processed according to JKR theory. The agreement was within measurement error provided the measurements were completed within an hour [32].

Table 2. DMW models parameters estimated from different durations of the relaxation data (holding phase only) for the 5Gel15Cream sample using spherical indentation. CV2 values may be compared with those in table 1.

Time (s)	10–20	10–50	10–100	10–300	CV2
C_0 (Pa)	1553.2	3265.9	3308.6	3116.4	0.2997
α_f	0.566	0.614	0.587	0.580	0.0488
τ_1 (s)	7.47	2.485	3.66	121.00	1.7314
τ_2 (s)	2.02	46.44	41.33	9.17	0.9053

For plate-compression, samples were removed from the mold carefully before testing and placed on a flat surface. The top surface of the sample was displaced $h_{\max} = 1$ mm toward the bottom surface at a ramp speed of 0.1 mm s^{-1} to give ramp times of $T_r = 10$ s. Samples were held for 300 s to measure stress relaxation.

We established the initial contact point of the plate with the sample surface as follows. In a preliminary step, we compressed the sample at very low constant speed (0.01 mm s^{-1}) before attempting the ramp relaxation test. A short-time moving-average filter was applied to the recorded force-versus-time curve to filter a small amount of load-cell noise as we detected the point at which the force first deviates from zero. We then positioned the probe at this point, waited at least 1 min to let the sample recover, and started the ramp-load relaxation experiment. Because the opposing sample surfaces were flat and parallel, this simple method provided a reproducible contact point.

Table 3. KVFD parameter estimates from different durations of the plate compression relaxation curve. Sample used is 5Gel15Cream. CV1 includes the initial 10 s ramp data and CV2 does not. Values shown are from measurements on one sample.

Time (s)	0–20	0–50	0–100	0–300	10–20	10–50	10–100	10–300	CV 1	CV 2
E_0 (Pa)	2019.7	2031.1	2029.6	2029.4	2089.3	2039.3	2032.0	2031.0	0.0026	0.0136
α	0.135	0.1360	0.1360	0.1360	0.134	0.135	0.135	0.136	0.0037	0.006
τ (s)	80.53	76.56	77.06	73.64	30.56	56.83	61.62	70.37	0.0367	0.3124

Table 4. DMW parameter estimates from different durations of the plate compression relaxation curve. Sample used is 5Gel15Cream. CV1 includes the initial 10 s ramp data and CV2 does not.

Time (s)	0–20	0–50	0 –100	0–300	10–20	10–50	10 –100	10–300	CV 1	CV 2
C_0 (Pa)	3902.0	3664.0	3521.0	3299.0	3333.1	3567.7	3558.2	3216.5	0.0704	1.410
α_f	0.646	0.329	0.293	0.314	0.239	0.194	0.192	0.277	0.0380	0.1371
τ_1 (s)	1.02	25.49	46.22	99.98	91.37	34.98	41.83	169.1	0.7335	0.9758
τ_2 (s)	10.59	2.04	4.39	7.22	46.57	31.97	22.54	20.03	0.3968	0.6087

3.3. Model fitting

3.3.1. Parameter estimation for the ramp-hold relaxation test and KVFD model. The ramp-hold relaxation curves for spherical indentation and plate compression tests were fitted to the KVFD analytical solutions of equations (6) and (8), respectively. For each relaxation curve, model parameters E_0, α, and τ were varied, and the set of parameters generating the least-squared error between model and data became the estimates. Parameters were initially selected manually to approximate the fit, which became the initial values for least-squares regression fits in MATLAB. The KVFD solutions for ramp relaxation curves describe the entire ramp-and-hold experimental time series. Thus any data segments from the curve should yield the same parameter estimation within numerical uncertainties. Due to noise in the experimental data, the least-squares fitting algorithm can truncate the search early if it becomes trapped in local optimal points. Manually selecting the initial values eliminated this problem.

It should be noted that for plate-compression tests only, there is a very small linear drift of the relaxation stress not explained by the model. A similar effect was reported in [34]. Drifting might be caused by instrument drift during measurements spanning 300 s or, more likely, as the assumed nonslip boundary conditions may have a small amount of friction that delays sample expansion during plate compression. We added the weak linear trend term $a{\cdot}t$ to the model after the 10 s ramp concluded to improve the quality of fit. Values for slope constant a were found to range between -0.004 and -0.001 in our experiments.

3.3.2. Parameter estimation for the ramp-hold relaxation test and DMW model. Parameters analogous to those of the KVFD set were obtained from a second-order Prony series assuming a Double Maxwell–arm Wiechert (DMW) model [28], yielding a relaxation modulus $G(t)$ given by

$$G(t) = C_0 + C_1 \exp(-t/\tau_1) + C_2 \exp(-t/\tau_2). \quad (10)$$

As others reported [28], there is no analytic solution for the time-varying force. If we analyze the relaxation curve during the holding phase only, we can assume the force $P_r(t)$ has a form similar to equation (10),

$$P_r(t) = B_0 + B_1 \exp(-t/\tau_1) + B_2 \exp(-t/\tau_2). \quad (11)$$

The ramp correction technique shown in equation (12) was adopted from the work of Mattice *et al* [28]. If the correction factor is defined by $\mathrm{RCF}_k = \frac{\tau_k}{T_r}(\exp(T_r/\tau_k) - 1)$, then model parameters can be corrected using

$$C_0 = \frac{B_0}{h_{\max}^{3/2}\left(8\sqrt{R}/3\right)}, \quad C_k = \frac{B_k}{(\mathrm{RCF}_k) h_{\max}^{3/2}\left(8\sqrt{R}/3\right)}. \quad (12)$$

This technique gives equations that relate B_k obtained by fitting equation (11) to relaxation data and C_k in equation (10). Two metrics derived from the model parameters: the infinite-time relaxation modulus $G(\infty)$ and fraction number α_f are calculated to compare with their KVFD counterparts E_0 and α for examining model stability under different experimental conditions. $G(\infty)$ is set equal to C_0 from equation (10), and α_f is defined as:

$$\alpha_f = 1 - \frac{G(\infty)}{G(0)} = \frac{\sum_{i=1}^{n} C_i}{C_0 + \sum_{i=1}^{n} C_i}. \quad (13)$$

3.3.3. Statistical metrics. The coefficient of determination R^2 was calculated to indicate the goodness of the fit between minimum least-squares model equations and the measured relaxation time series. In the next section, we vary the duration of the relaxation curve included in the fitting process to observe changes in model parameter estimates for KVFD and DMW models. Comparisons were made by computing the coefficients of variation (CV). CV is defined as the standard deviation of parameter estimates for equivalent gel samples divided by the mean parametric value. Two-sided Students T-test was applied to determine whether spherical indentation and plate compression testing on the same samples yielded statistically equivalent parameter estimates.

4. Results

There are no established standards for calibrating viscoelastic measurements in soft materials, although comparisons among independent measurement techniques can test for precision

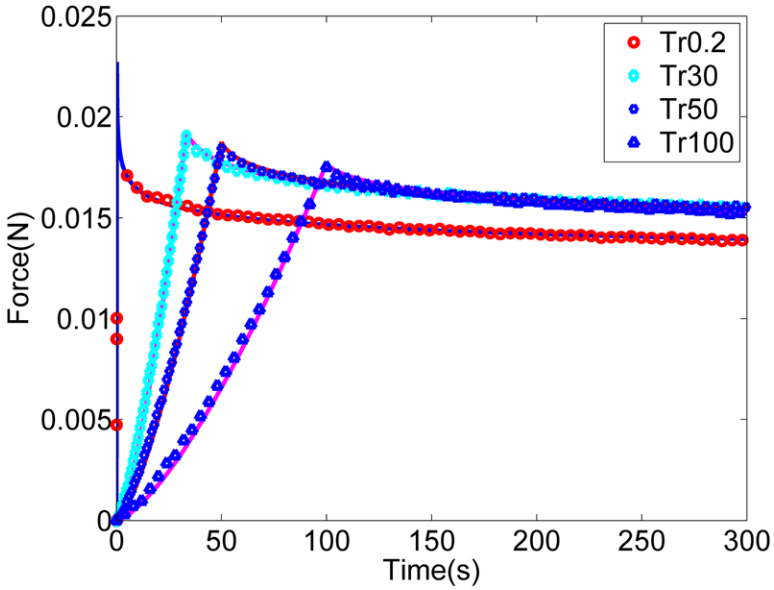

Figure 3. Illustration of KVFD model fits to data from 5Gel15Cream samples acquired using ramp times between 0.2 and 100 s. Points plotted are experimental relaxation data and the curves use the best-fit KVFD model-based solutions. Experimental data are down sampled by factors of 10–50 in the ramp phase and 120 in the holding phase for display purposes.

and consistency [32]. A model-based solution can be valuable for predicting viscoelastic properties from load-relaxation time series if it satisfies the following coupled criteria: (1) The model reliably predicts sample responses with few parameters; (2) Parameter estimates are robust to changes in experimental variables and conditions; (3) The same model applies to different materials having a variety of mechanical properties in a range of interest.

In this study, we approached validation of the KVFD model solution for a ramp-hold relaxation test by first identifying a stable, reproducible, viscoelastic material. We then made a series of measurements varying several key experimental parameters and observed the variability of KVFD model parameters, (E_0, α, τ). The precision of estimates was examined by comparing KVFD results to those of the DMW model using spherical indentation and plate compression testing over a range of experimental variables. We also varied the material properties of the test samples within a small range of soft biological tissues to test model applicability.

4.1. Impact of relaxation time on the variability of estimated model parameters

For this study, the sample labeled 5Gel15Cream (5% gelatin, 15% cream, 80% water) is subjected to a force/stress relaxation test. The ramp time T_r is fixed at 10 s for both spherical indentation and plate compression. Figure 2 gives an example of the relaxation data from spherical indentation and the best fit to the model given by equation (6). The four time durations studied are indicated on the time axis in figure 2.

4.1.1. Spherical indentation. Parameter values are estimated by fitting the KVFD ramp solution to different time durations of the relaxation data. Results are listed in table 1. The coefficient of variation (CV) reflects the reproducibility of the fitting results for the different durations indicated in the first row of the table. CV1 represents the variability of fitting the ramp and the holding phase of the force–measurement time series up to the time indicated, and CV2 represents the variability of fitting only the holding phase, which begins at 10 s.

Table 5. Coefficient of determination R^2 for goodness fitting measurement of 5Gel15Cream sample and the KVFD model.

T_r (s)	0.2	2	10	20	33	50	100
R^2	0.968	0.979	0.988	0.988	0.988	0.989	0.988

First, we find there is no significant change in α when model fitting the holding phase at various durations with or without the initial 10 s of ramp data. α is the most stable material parameter in this study; it is robust to variations in experimental parameters. Second, the elastic modulus E_0 has the lowest coefficient of variation when the ramp data is included in the fit (CV1). Also, including the ramp phase, we find that modulus estimates decrease about 4%. Similarly, time constant estimates τ are most precise when the ramp data are included in the fitting procedure, and excluding the ramp biases τ estimates. Noise in the recording of the time-varying force means that curve-fitting results may not be unique; the best fits are strongly influenced by the initial values supplied to the regression. We believe that by including the ramp time in the fitting procedure, the chance of finding that one parameter set that best describes the entire time period is increased, thus the parameters generated are less dependent on the duration of the force data.

Fitting the DMW model to the same relaxation data, we find the results summarized in table 2. Because there is no analytic solution for ramp loading, only the holding phase was fitted to equation (11). Model parameters are found for ramp indentation using equations (12) and (13).

Among the DMW parameters, α_f stands out as relatively stable, however the other parameters are sensitive to the duration of the relaxation data selected for inclusion in model fitting. Compared with KVFD model parameters E_0, α, and τ

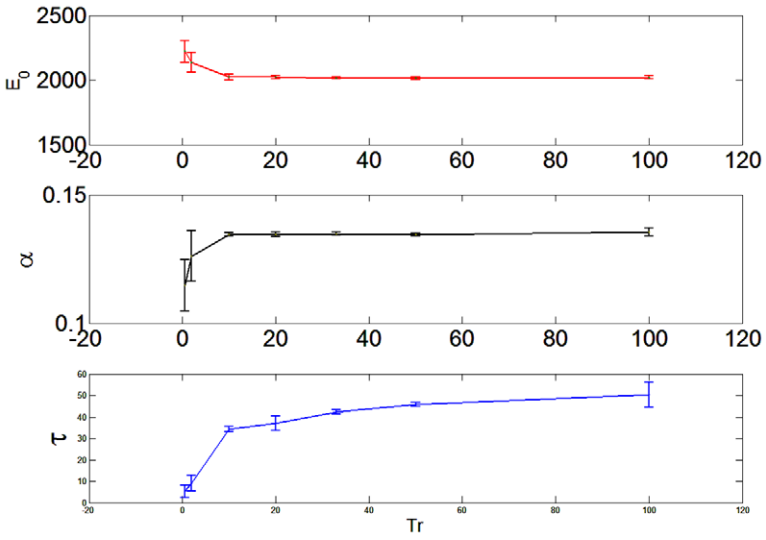

Figure 4. Estimated parameters for the 5Gel15Cream sample measured for different ramp times, T_r. Measurements are indicated by the mean points ± 1 sd. Means are averaged over data from three samples. Lines are added only to clarify trends.

parameters, DMW parameters C_0, α_f and time constants τ_1 and τ_2 have CVs that are 4–30 times larger. Greater estimation precision indicates a uniqueness of the KVFD solution across the entire measurement time. In summary, the KVFD ramp solution for spherical indentation (equation (6)) reliably and precisely describes the entire relaxation time series with less parametric variability that the DMW model. Including the ramp portion of the relaxation data improves the fit, which yields more precise model parameter estimates. We cannot expect the two models to give the same values, but we do expect the estimates for each model to be independent of the duration of the data used in the model fitting procedures.

4.1.2. Plate compression. The analysis was repeated for plate compression on 5Gel15Cream samples. Parameter estimates are found from the solution derived for the KVFD model and plate compression geometry in equation (8). These results are listed in table 3. For comparison, fitted results using the DMW model also for plate compression and the same durations of relaxation data are summarized in table 4. Note that the analytical solution for the DMW model during the ramp loading period can be derived for plate compression but not spherical indentation.

From the data in tables 3 and 4, we again find the KVFD model parameters are much more stable with respect to the duration of the relaxation curve when compared with those of the DMW model. Notice too that the KVFD model has fewer and more precisely estimated parameters, which offer major advantages when these parameters are mapped into elasticity image data provided contrast is also transferred with high fidelity.

4.2. Impact of ramp time T_r on model parameter estimates

T_r should not influence parametric estimates provided the model fits the measurements equally well over a practical range of applied indention speeds. For spherical indentation, we applied a strain of 0.05 over a range from 0.2 to 100 s. Below a T_r threshold value, quickly deforming the sample to approximate a step function is likely to create an underdamped response in the instrument that is not accounted for by the model. The variability of parameters estimated from the KVFD ramp solution for ramp durations between 0.2 and 100 s are repeated on several 5Gel15Cream samples. We waited at least 30 min between measurements for samples to fully recover before the next test. All measurements were made on three 5Gel15Cream samples from the same batch.

Figure 3 shows the fitting results for T_r values of 0.2 s, 33 s, 50 s and 100 s. The R^2 metric for the same ramp times are found in table 5, which shows the data are well described by the best-fit model especially for $T_r \geqslant 10$ s. R^2 will not equal 1 because of signal-independent noise in the time-varying force measurements. These results suggest that material properties are not strain-rate dependent in this range and the model consistently accounts for the force relaxation occurring during the ramp deformation.

It is expected that all of the curves in figure 3 will converge at large relaxation times because the elastic modulus at infinite time $G(\infty)$ is equal to E_0 in the KVFD model, which does not depend on T_r. As shown in figure 3, relaxation curves for different ramp times tend to converge for relaxation time >250 s except at $T_r = 0.2$ s, suggesting the step-relaxation response is biased by the measurement process.

The stability of the three KVFD parameter estimates can be assessed from the plots of figure 4. When T_r is between 10–50 s, all three parameters are influenced very little by T_r. Among all 3 parameters, α has the smallest CV because it is only sensitive to the shape of the relaxation curve, whereas E_0 is influenced by the amplitude that depends on the initial contact between the probe and the sample surface. Variability in initial contact is well known to cause uncertainty in model-parameter estimates. α is the most stable parameter, while τ is significantly more dependent on T_r compared with E_0 and α.

Very small T_r can approximate a step deformation. However, indenting at high probe velocity introduces uncertainties from instrument oscillations. As shown in figure 4 when $T_r \leqslant 10$ s,

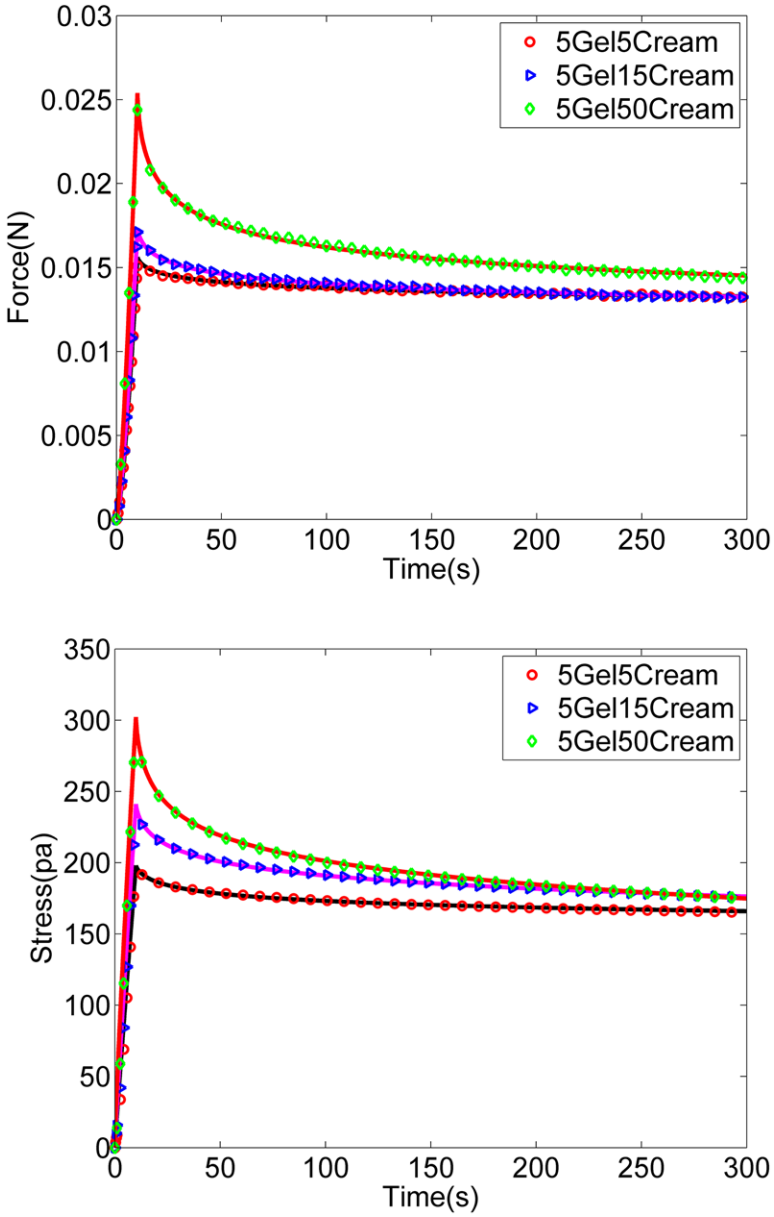

Figure 5. Spherical indention (top) and plate compression (bottom) test measurements (points) along with best-fit KVFD solutions (lines). The three curves correspond to the samples listed in the legend. The experimental curve is down sampled by a factor of 5–10 in the ramp phase and 100–150 in the holding phase.

estimated parameters deviate from values obtained at longer ramp times where a plateau is reached.

Ramp deformations are preferred over steps; nevertheless, measurements should be made over a range of T_r when investigating different sample types to ensure a plateau is reached. If T_r is too long, the measurement system might drift or sample properties might change. For this emulsion, parameter estimates are stable for $10 \leqslant T_r \leqslant 50$ s. Others also found that short-ramp relaxation data fit to a step-relaxation solution can result in big parameter errors [28, 33].

4.3. Samples with varying properties

In the above two sections, we studied the stability of parameters estimated by the KVFD and DMW models of ramp relaxation data on one type of sample (5Gel15Cream). In this section, samples with different viscosities are examined for different stress–strain probe geometries.

Samples with three different cream concentrations (5%, 15%, 50%) and the same gelatin concentration (5%) were constructed. 3–5 samples from the same batch of each material type were prepared for analysis. The entire recorded time series including the ramp phase were fitted to the proposed ramp solutions. Figure 5 shows examples of experimental relaxation curves and corresponding model predictions for each sample concentration for tests using spherical indentation (top) and plate compression (bottom). The models represent the experimental data very well; i.e. $R^2 \geqslant 0.98$.

Table 6 contains the numerical values of model parameters from spherical indentation and plate compression tests. The

Table 6. Comparison of parameter estimates from spherical indentation and plate compression testing using the KVFD model and emulsion samples with cream concentrations of 5%, 15%, and 50% to vary the viscosity. The mean value for measurements obtained on 3–5 samples at each cream concentration are shown and the error bars are ±1 sd.

Sample		5%	15%	50%
Spherical indention tests	E_0	1782.51 ± 53.20	2020.92 ± 28.31	1952.51 ± 20.62
	α	0.0768 ± 0.002	0.135 ± 0.001	0.209 ± 0.002
	τ	38.69 ± 19.82	34.31 ± 13.61	150.6741 ± 11.48
Plate compression tests	E_0	1754.90 ± 56.61	2029.30 ± 57.73	1942.31 ± 32.12
	α	0.0798 ± 0.002	0.136 ± 0.005	0.216 ± 0.007
	τ	47.56 ± 21.21	68.80 ± 36.06	159.46 ± 15.77

results for the two geometries agree within one standard deviation of the measurement. Students T-test suggested that the two measurements have no significant difference for all cream concentrations at the 0.05 significance level. The high consistency of estimates comparing two testing geometries further confirms the reliability of utilizing the ramp solution of the KVFD model to describe viscoelastic properties.

5. Discussion

Experimental error contributes uncertainty to model parameter estimates. Except for the random error from force/displacement sensors, parameter uncertainty could originate from several sources in this study.

First, inaccuracies in recording indentation depth $h_{\max}$ can add significant bias to parameter estimations, especially E_0. Unlike stiff materials, it is challenging to identify the moment of first contact with the indenter probe when studying soft, wet tissue-like materials. Any deviation from the exact indention depth, including surface roughness, biases E_0.

Second, errors occur as part of the fitting process. Least-squares fitting of experimental data to model functions is challenging because of noise in the force measurements, which enables the regression algorithm to settle into local minima rather than the global minimum that we hope to find. The problem is amplified as the number of model parameters increases. Experience enabled us to select model parameters when initiating numerical searches that were close to those giving a global minimum error. Fitting the full duration of the ramp-hold relaxation curve yields more precise parameter estimates by avoiding local minima traps. Also, the concise feature set of the KVFD model coupled with the ramp-hold stimulus leads to more reliable parameter estimates.

Third, despite our best efforts to manufacture uniform test materials reproducibly, there remains variations in material properties within and among the samples tested. The mechanical properties of hydrogels are affected by the details of thermal history, including manufacturing temperature, heating duration, cooling rates and time and temperature at which the cream is added. The fact that gelatin stiffness varies over time when chemical cross linkers are not used and with pH further makes the sample elastic modulus vulnerable to measurement variations [35]. We were aware of these influences and made every effort to minimize all material property variations by standardizing the sample manufacturing process.

Finally, the boundary conditions of the sample are another common source of variation in indentation testing of soft materials. Inner-sample stress variations near stiff or soft boundaries influence force measurements. The general rule of thumb for spherical indentation is for the diameter of the probe to be less than one tenth of the sample diameter. We confirmed the validity of this rule for representative gelatin samples recently [32]. Indented samples were 50 mm in diameter for a 5 mm probe diameter.

We verified that T_r does not produce significant changes in model parameter estimates provided T_r is larger than 10 s in these emulsion samples. Including the ramp deformation, model fits involving force/stress relaxation data from 50–300 s in duration yield equivalent results.

Samples were deformed using two geometries in this study: spherical indentation and plate compression. Each has advantages under different situations. The spherical indenter minimizes the effects of irregular sample geometries and has fewer boundary effects as long as the diameters of the samples are much larger than indenter. Spherical indentation also has no strict requirement on surface flatness, as long as a small flat region can be found. It is widely used to characterize viscoelastic materials. However, depending on the dynamic range of the load cell, spherical indentation may not be ideal for very soft materials (<3 kPa) as the contact area is too small to generate sufficient force to avoid significant quantization errors in digital force measurements. In contrast, plate compression increases the net force in soft materials, using more of the dynamic range of the sensor, but requires the sample surface to be very flat. Also sample area and height must be precisely measured since they strongly influence stress and strain calculations. Moreover, plate compression of samples induces a small drift in relaxation force over time when the frictional forces at the sample-plate surface are non-uniform. The choice between the two geometries depends on sample properties, where spherical indentation is preferred except for very soft samples.

6. Conclusion

Closed-form solutions for ramp-relaxation testing of soft viscoelastic materials involving the KVFD model give precise estimates of model parameters for spherical indention and plate compression within a broad range of experimental conditions. These parameters can be interpreted in terms of viscoelastic

properties of the material. Step deformation experiments should be avoided when possible. The consistency of results shown in this report suggests that experimentally independent estimates are possible by fitting models to measurements spanning the entire force-relaxation time series. Other rheological models should be explored, but our results suggest the ramp-relaxation experiment combined with the concise parameter set of the KVFD model offers much estimation stability and precision. Since there are no standard materials for calibrating relaxation measurements, we cannot claim to measure intrinsic material properties. Nevertheless, the high precision and independence of the results on experimental parameters suggests this approach offers advantages for mechanical measurements of soft materials in the elastic modulus range of many soft tissues (<10 kPa) where precise measurements can be difficult to achieve.

Acknowledgments

This study was supported by the China Scholarship Council and by the National Cancer Institute of the US National Institute of Health under award number ROI CA168575. The content is solely the responsibility of the authors and does not necessarily represet the official views of the National Institutes of Health. The authors gratefully acknowledge a generous supply of gelatin provided Rousselot Inc., Dubuque IA. The work was carried out at the Department of Bioengineering and Beckman Institute for Advanced Science and Technology, University of Illinois at Urbana-Champaign, Urbana IL, 61801, USA

Appendix

A.1. Spherical indenter, ramp-hold relaxation solution for KVFD model

Using the Boltzmann integral expression for spherical indentation under distance control, the relaxation force response is given by

$$P_r(t) = \frac{8\sqrt{R}}{3}\int_0^t G(t-\tau)\frac{\mathrm{d}\left[h^{\frac{3}{2}}(\tau)\right]}{\mathrm{d}\tau}\mathrm{d}\tau. \tag{A.1}$$

The relaxation modulus for KVFD model is

$$G(t) = E_0 + \eta\frac{t^{-\alpha}}{\Gamma(1-\alpha)},\quad 0<\alpha<1. \tag{A.2}$$

From (A.1) and (A.2), we can obtain

$$P_r(t) = \frac{8\sqrt{R}}{3}\int_0^t\left(E_0+\eta\frac{(t-\tau)^{-\alpha}}{\Gamma(1-\alpha)}\right)\frac{\mathrm{d}\left[h^{\frac{3}{2}}(\tau)\right]}{\mathrm{d}\tau}\mathrm{d}\tau. \tag{A.3}$$

The ramp displacement condition can be expressed by

$$h(t) = \begin{cases} k\cdot t & 0\leqslant t\leqslant T_r \\ h_0 = k\cdot T_r & t\geqslant T_r. \end{cases} \tag{A.4}$$

By combining (A.3) and (A.4), we obtain

$$P_r(t) = \begin{cases} \frac{8\sqrt{R}}{3}\int_0^t\left(E_0+\eta\frac{(t-\tau)^{-\alpha}}{\Gamma(1-\alpha)}\right)\cdot\frac{3}{2}k^{\frac{3}{2}}\tau^{\frac{1}{2}}\mathrm{d}\tau & 0\leqslant t\leqslant T_r \\ \frac{8\sqrt{R}}{3}\left(\int_0^{T_r}\left(E_0+\eta\frac{(t-\tau)^{-\alpha}}{\Gamma(1-\alpha)}\right)\cdot\frac{3}{2}k^{\frac{3}{2}}\tau^{\frac{1}{2}}d\tau+\int_{T_r}^t 0\cdot\mathrm{d}\tau\right) & t\geqslant T_r. \end{cases} \tag{A.5}$$

(1) For $0\leqslant t\leqslant T_r$, let $\xi=\frac{\tau}{t}$. Then

$$\int_0^t(t-\tau)^{\beta}\tau^{\frac{1}{2}}\mathrm{d}\tau = \int_0^1 t^{\beta}(1-\xi)^{\beta}t^{\frac{1}{2}}\xi^{\frac{1}{2}}t\mathrm{d}\xi = t^{\frac{3}{2}+\beta} \times\int_0^1\xi^{\frac{1}{2}}(1-\xi)^{\beta}\mathrm{d}\xi = t^{\frac{3}{2}+\beta}B\left(\frac{3}{2},\beta+1\right), \tag{A.6}$$

where $B(x,y)=\int_0^1 t^{x-1}(1-t)^{y-1}\mathrm{d}t\quad \mathrm{Re}(x)>0,\mathrm{Re}(y)>0$ is a Beta function. Thus from (A.5) and (A.6), and letting $\beta=-\alpha$, we obtain

$$P_r(t) = 4\sqrt{R}k^{\frac{3}{2}}\left(\frac{2}{3}E_0t^{\frac{3}{2}}+\frac{\eta}{\Gamma(1-\alpha)}t^{\frac{3}{2}-\alpha}B\left(\frac{3}{2},1-\alpha\right)\right) = 4\sqrt{R}k^{\frac{3}{2}}E_0\,t^{\frac{3}{2}}\left(\frac{2}{3}+\frac{1}{\Gamma(1-\alpha)}\left(\frac{t}{\tau}\right)^{-\alpha}B\left(\frac{3}{2},1-\alpha\right)\right). \tag{A.7}$$

(2) For $t\geqslant T_r$, let $\xi=\frac{\tau}{T_r}$. Then

$$\int_0^{T_r}(t-\tau)^{\beta}\tau^{\frac{1}{2}}\mathrm{d}\tau = \int_0^1 t^{\beta}\left(1-\xi\frac{T_r}{t}\right)^{\beta}\left(\xi\frac{T_r}{t}\right)^{\frac{1}{2}}t^{\frac{3}{2}}d\left(\xi\frac{T_r}{t}\right). \tag{A.8}$$

Letting $\zeta=\xi\frac{T_r}{t}$, we find

$$\int_0^{T_r}(t-\tau)^{\beta}\tau^{\frac{1}{2}}\mathrm{d}\tau = \int_0^{\frac{T_r}{t}}t^{\frac{3}{2}+\beta}\zeta^{\frac{1}{2}}(1-\zeta)^{\beta}\mathrm{d}\zeta = t^{\frac{3}{2}+\beta} \times B\left(\frac{T_r}{t};\frac{3}{2},\beta+1\right), \tag{A.9}$$

where, $B(x;a,b)=\int_0^x t^{a-1}(1-t)^{b-1}\mathrm{d}t$ is the incomplete Beta function.

Thus from (A.5) and (A.9), and letting $\eta=E_0\tau^{\alpha}$, we obtain

$$P_r(t) = 4\sqrt{R}k^{\frac{3}{2}}\left(\frac{2}{3}E_0T_r{}^{\frac{3}{2}}+\frac{\eta}{\Gamma(1-\alpha)}t^{\frac{3}{2}-\alpha}B\left(\frac{T_r}{t};\frac{3}{2},1-\alpha\right)\right) = 4\sqrt{R}k^{\frac{3}{2}}E_0T_r{}^{\frac{3}{2}}\left(\frac{2}{3}+\frac{1}{\Gamma(1-\alpha)}\left(\frac{t}{T_r}\right)^{\frac{3}{2}}\left(\frac{t}{\tau}\right)^{-\alpha}B\left(\frac{T_r}{t};\frac{3}{2},1-\alpha\right)\right). \tag{A.10}$$

Combining (A.7) and (A.10), the ramp-hold relaxation solution is

$$P_r(t) = \begin{cases} 4\sqrt{R}k^{3/2}E_0t^{3/2}\left[\frac{2}{3}+\frac{(t/\tau)^{-\alpha}}{\Gamma(1-\alpha)}B\left(\frac{3}{2},1-\alpha\right)\right], & 0<t\leqslant T_r \\ 4\sqrt{R}k^{3/2}E_0T_r{}^{3/2}\left[\frac{2}{3}+\frac{\left(\frac{t}{T_r}\right)^{3/2}\left(\frac{t}{\tau}\right)^{-\alpha}}{\Gamma(1-\alpha)}B\left(\frac{T_r}{t};\frac{3}{2},1-\alpha\right)\right], & t\geqslant T_r. \end{cases} \tag{A.11}$$

References

[1] VanLandingham M R 2003 *Review of Instrumented Indentation* National Inst Of Standards and Technology Gaithersburg MD

[2] Palacio-Torralba J, Hammer S, Good D W, McNeill S A, Stewart G D, Reuben R L and Chen Y 2015 Quantitative diagnostics of soft tissue through viscoelastic characterization using time-based instrumented palpation *J. Mech. Behav. Biomed. Mater.* **41** 149–60

[3] Park S W and Schapery R A 1999 Methods of interconversion between linear viscoelastic material functions: I. A numerical method based on Prony series *Int. J. Solids Struct.* **36** 1653–75

[4] Murata H, Shigeto N and Hamada T 1990 Viscoelastic properties of tissue conditioners—stress relaxation test using Maxwell model analogy *J. Oral Rehabil.* **17** 365–75

[5] Sedef M, Samur E and Basdogan C 2006 Real-time finite-element simulation of linear viscoelastic tissue behavior based on experimental data *IEEE Comput. Graph. Appl.* **26** 58–68

[6] Jagota A, Argento C and Mazur S 1998 Growth of adhesive contacts for Maxwell viscoelastic spheres *J. Appl. Phys.* **83** 250–9

[7] Clayton E H, Garbow J R and Bayly P V 2011 Frequency-dependent viscoelastic parameters of mouse brain tissue estimated by MR elastography *Phys. Med. Biol.* **56** 2391–406

[8] Caputo M, Carcione J M and Cavallini F 2011 Wave simulation in biologic media based on the Kelvin–Voigt fractional-derivative stress–strain relation *Ultrasound Med. Biol.* **37** 996–1004

[9] Kiss M Z, Varghese T and Hall T J 2004 Viscoelastic characterization of *in vitro* canine tissue *Phys. Med. Biol.* **49** 4207–18

[10] Teodorovich E V 1978 Sliding of a cylinder on a viscoelastic foundation *J. Appl. Math. Mech.* **42** 384–9

[11] Golden J M 1979 The problem of a moving rigid punch on an unlubricated visco elastic half-plane *Q. J. Mech. Appl. Math.* **32** 25–52

[12] Golden J M 1982 Approximate analytic treatment of the problem of a moving ellipsoidal punch on a viscoelastic half-space *Q. J. Mech. Appl. Math.* **35** 155–71

[13] Flugge W *1967 Viscoelasticity* (Waltham, MA: Blaisdell Publishing Company)

[14] Christensen R M 1982 *Theory of Viscoelasticity: an Introduction* (New York: Academic)

[15] Pipkin A 1972 *Lectures on Viscoelasticity Theory. Applied Mathematical Sciences* (Berlin: Springer)

[16] Friedrich Ch, Sehiessel H and Blumen A 1999 Constitutive behavior modeling and fractional derivatives *Rheol. Ser.* **12** 429–66

[17] Koeller R C 1984 Applications of fractional calculus to the theory of viscoelasticity *J. Appl. Mech.* **51** 299–307

[18] Papoulia K D, Panoskaltsis V P, Kurup N V and Korovajchuk I 2010 Rheological representation of fractional order viscoelastic material models *Rheol. Acta* **49** 381–400

[19] Sasso M, Palmieri G and Amodio D 2011 Application of fractional derivative models in linear viscoelastic problems *Mech. Time-Dependent Mater.* **15** 367–87

[20] Taylor L S, Lerner A L, Rubens D J and Parker K J 2002 A Kelvin–Voight fractional derivative model for viscoelastic characterization of liver tissue *ASME 2002 Int. Mechanical Engineering Congress and Exposition* (American Society of Mechanical Engineers) pp 447–8

[21] Zhuravkov M A and Romanova N S 2014 Review of methods and approaches for mechanical problem solutions based on fractional calculus *Math. Mech. Solids* **5** 1–26

[22] Di Paola M, Pirrotta A and Valenza A 2011 Visco-elastic behavior through fractional calculus: an easier method for best fitting experimental results *Mech. Mater.* **43** 799–806

[23] Meral F C, Royston T J and Magin R 2010 Fractional calculus in viscoelasticity: an experimental study *Commun. Nonlinear Sci. Numer. Simul.* **15** 939–45

[24] Magin R L 2012 Fractional calculus in bioengineering: a tool to model complex dynamics *13th Int. Carpathian Control Conf. (ICCC), 2012* (IEEE) pp 464–9

[25] wJ Welch S, Rorrer R A and Duren R G Jr 1999 Application of time-based fractional calculus methods to viscoelastic creep and stress relaxation of materials *Mech. Time-Dependent Mater.* **3** 279–303

[26] Lee S and Knauss W G 2000 A note on the determination of relaxation and creep data from ramp tests *Mech. Time-Dependent Mater.* **4** 1–7

[27] Abramowitch S D and Woo S L-Y 2004 An improved method to analyze the stress relaxation of ligaments following a finite ramp time based on the quasi-linear viscoelastic theory *J. Biomech. Eng.* **126** 92–97

[28] Mattice J M, Lau A G, Oyen M L and Kent R W 2006 Spherical indentation load-relaxation of soft biological tissues *J. Mater. Res.* **21** 2003–10

[29] Tzikang C 2000 Determining a Prony series for a viscoelastic material from time varying strain data NASA Technical Publication: NASA / TM-2000–210123, ARL-TR-2206

[30] Mainardi F 1991 Fractional calculus: some basic problems in continuum and statistical mechanics *Fractals and Fractional Calculus in Continuum Mechanics* (Vienna: Springer) vol 378 pp 291–348

[31] Podlubny I 1998 *Fractional Differential Equations: an Introduction to Fractional Derivatives, Fractional Differential Equations, to Methods of their Solution and Some of their Applications* vol 198 (New York: Academic) eBook ISBN: 9780080531984

[32] Altahhan K N, Wang Y, Sobh N and Insana M F 2015 Indentation measurements to validate dynamic elasticity imaging methods *Ultrason. Imag.* **pii** 15

[33] Oyen M L 2005 Spherical indentation creep following ramp loading *J. Mater. Res.* **20** 2094–100

[34] Cai S, Hu Y, Zhao X and and Suo Z 2010 Poroelasticity of a covalently crosslinked alginate hydrogel under compression *J. Appl. Phys.* **108** 113514

[35] Yapp R D and Insana M F 2009 pH-induced contrast in viscoelasticity imaging of biopolymers *Phys. Med. Biol.* **54** 1089

[36] Kalyanam S, Yapp R D and Insana M F 2009 Poroviscoelastic behavior of gelatin hydrogels under compression: implications for bioelasticity imaging *ASME J. Biomech. Eng.* **13** 081005